Domain formation and strain relaxation in epitaxial ferroelectric heterostructures

B. S. Kwak* and A. Erbil†
School of Physics, Georgia Institute of Technology, Atlanta, Georgia 30332

J. D. Budai, M. F. Chisholm, and L. A. Boatner
Solid State Division, Oak Ridge National Laboratory, Oak Ridge, Tennessee 37831-6056

B. J. Wilkens‡
Bell Communications Research, Red Bank, New Jersey 07701-7020
(Received 22 November 1993)

The growth of $PbTiO_3$ films by a metalorganic chemical-vapor-deposition technique has resulted in three-dimensionally epitaxial heterostructures on various single-crystal substrates. These heterostructures consist of $PbTiO_3$ films on the (001) surface of the single crystals: potassium tantalate ($KTaO_3$), strontium titanate ($SrTiO_3$), and magnesium oxide (MgO). It was found that the presence of a structural (ferroelectric) phase transition in $PbTiO_3$ leads to a "strain-accommodating" mechanism in which a domain pattern forms as the system cools through the Curie temperature and limits the extension of interfacial strain in the heterostructure—thus minimizing the total energy of the heterostructure. For $PbTiO_3/KTaO_3(001)$, the interfacial strain is accommodated by the formation of a periodic domain pattern in the overlayer. In $PbTiO_3/SrTiO_3(001)$, which exhibits an excellent lattice match between respective *a* lattice parameters, the film exists as a single *c* domain. The $PbTiO_3$/MgO(001) system, having a poor lattice match for both the *a* and *c* axes, appears to find the energy minimum by locking into domains of two-dimensional superlattices with the greatest atomic coincidences. It is found that the nature of the domain pattern depends very strongly on both the film thickness and measuring temperature. A theoretical model of the domain-pattern formation has been developed by using linear-elasticity theory and a Landau-Ginzburg-Devonshire-type phenomenological theory for the substrate and the overlayer, respectively. The theoretical predictions and the experimental measurements were in good agreement in both the thickness and temperature dependence of the relative domain population and the spontaneous strains.

I. INTRODUCTION

Heterostructures fabricated using a variety of semiconducting materials have been extensively investigated during the past two decades due to a high level of interest in the development of device applications for such systems and in the opportunities they offer for the study of fundamental issues in interface physics and the mechanisms of thin-film growth.[1] Heterostructures of materials other than semiconductors (e.g., metals, insulators, superconductors, and ferroelectrics), on the other hand, have not been as extensively investigated—although the practical and fundamental potential of such systems is high, as demonstrated recently in the case of metal-semiconductor heterostructures.[2] While the study of heterostructures of metal oxides is still in the early stages of development, such systems have recently emerged as one of the most important classes of heterostructures. This emergence has been driven in part by the many important physical phenomena recently observed in these systems including high-T_c superconductivity in the copper-oxide-based compounds.[3,4] Progress in this area has been relatively slow, however, because of difficulties in the growth of these materials with high crystalline quality and known defect structures.

In the present work, $PbTiO_3$ is employed as a prototype system because of its simple perovskite structure.[5] Many compounds of this type undergo one or more structural phase transitions, and, in fact, $PbTiO_3$ undergoes a cubic-to-tetragonal ferroelectric phase transition at around 770 K.[6] This material also has a large spontaneous polarization and a relatively small dielectric constant.[6] Numerous potentially important applications of lead titanate and other ferroelectric oxides in the field of electronics and optoelectronics have recently been reviewed.[7,8]

One of the most important issues in the study of heterostructures is the nature of the film-substrate interaction. Film-substrate interactions may produce interfacial defects (e.g., misfit dislocations), pseudomorphic growth, and domain formation, resulting in film structures and properties that are profoundly different from those of the bulk phase.[9] In particular, film-substrate interactions can modify the final structure and properties of the film in epitaxial heterostructures. For the case of polycrystalline films, however, the final film structure and properties are not so drastically different from those of the bulk, presumably due to the presence of strain-releasing centers such as grain boundaries or misfit dislocations.

Epitaxy is the overgrowth of a crystalline thin film on a single-crystal substrate with a definite orientation relative to and determined by the crystallographic lattice of the

0163-1829/94/49(21)/14865(15)/$06.00

substrate. Equilibrium theories of epitaxy[10,11] predict that, below a critical thickness, lattice mismatch between a substrate and a thin film is accommodated entirely by the strain in the film. Above this thickness, the strain in the film would be partially relieved by misfit dislocations. If the film undergoes a structural phase transition from a high-symmetry phase to a low-symmetry phase during cooling from the growth temperature, however, the bulk epitaxial strain can be relieved by domain formation as suggested by Roitburd[12] and Bruinsma and Zangwill.[9] This effect is reminiscent of the formation of coherent alternating twins in martensites.[12,13] In a recent paper,[14] we have reported on a specific epitaxial multidomain system, namely, a ferroelectric lead titanate ($PbTiO_3$) thin film deposited on a single-crystal potassium tantalate ($KTaO_3$) substrate, as an experimental realization of this type of structure. It was reported that the domain structure of the thin films depended very strongly on both the film thickness and the measurement temperature.

In the present work, we expand upon our initial report[14] and provide more complete information on both the theoretical model and the experimental results for the phenomenon of domain formation. This work encompasses both the description of the nature of the three-dimensional epitaxy and a detailed comparison between the theoretical model and the experimental results. In the theoretical model of this phenomenon, we use linear-elasticity and a Landau-Ginzburg-Devonshire type phenomenological theory for the substrates and overlayer, respectively. In addition to $PbTiO_3/KTaO_3$ (001), we consider $PbTiO_3$ on (001) surfaces of single crystals of strontium titanate ($SrTiO_3$) and magnesium oxide (MgO). These different substrates allow us to explore the effects of various lattice and thermal-expansion mismatches. The structural parameters and thermal-expansion coefficients for the materials studied here are given in Table I.

At zero stress $KTaO_3$ retains the prototype cubic-perovskite structure down to the very lowest temperatures—although it is just barely stable against a ferroelectric transition near 4 K.[5] $SrTiO_3$ also has a perovskite structure and undergoes a nonferroelectric displacive phase transition at ~105 K.[5] MgO, on the other hand, has the cubic NaCl structure at all temperatures. Thus, at the growth temperature of 823 K, the $PbTiO_3$ thin film and all of the substrates considered here are in the cubic phase. Upon cooling to room temperature from the deposition temperature, only the $PbTiO_3$ film undergoes a ferroelectric phase transition. The formation of domains in the ferroelectric phase will be shown to limit the extension of the strain field to a distance comparable to the domain-wall periodicity in the substrate, thereby reducing the bulk-epitaxial strain energy. This effect is analogous to the formation of domain walls in ferromagnets which minimize the magnetic energy near the free surface.[15]

The $PbTiO_3$ thin films have been grown by using the metalorganic chemical-vapor-deposition (MOCVD) technique which is currently the primary growth technique for the formation of thin films of compound semiconductors.[17] Its dominance in this area is, of course, due to the advantages of MOCVD over other deposition techniques. Among the advantages of MOCVD are (1) flexible and easy control of growth parameters, (2) generally higher vapor pressures of metalorganics, (3) low-temperature processing, (4) ideal adaptability to multicomponent and layer deposition, and (5) easy scale up to commercial production. Some preliminary reports of investigations of the MOCVD growth of the oxides mentioned above have appeared recently.[18,19]

In Sec. II, the experimental aspects of the work, including the thin-film deposition and characterization techniques, are presented. Section III describes the nature of the three-dimensional epitaxy for all three heterostructures, i.e., $PbTiO_3$ on $KTaO_3$(001), $SrTiO_3$(001), and MgO(001). Section IV provides a detailed treatment of the theoretical model developed here, where the total-energy functional for the heterostructure $PbTiO_3$ on $KTaO_3$(001) is derived. In Sec. V, the theoretical and experimental results for the thickness and temperature dependence are compared. Finally, Sec. VI provides concluding remarks including suggestions for future related investigations.

TABLE I. Structural parameters (given in Å) and thermal-expansion coefficients (TEC) of various materials are listed (Ref. 16). The value of the TEC for $PbTiO_3$ is for the extrapolated line of the cubic phase.

	Structural parameters				TEC[a]
	Room temperature		Growth temperature		
Materials	Crystal structure	Bulk lattice constants	Crystal structure	Bulk lattice constants	
$PbTiO_3$	tetragonal	$a=3.899$ $c=4.153$	cubic	$a=3.986$	12.6×10^{-6}
$KTaO_3$	cubic	$a=3.989$	cubic	$a=4.003$	6.67×10^{-6}
$SrTiO_3$	cubic	$a=3.905$	cubic	$a=3.928$	11.7×10^{-6}
MgO	cubic	$a=4.213$	cubic	$a=4.239$	14.8×10^{-6}

[a]Reference 16.

II. EXPERIMENTAL METHODS

A. Thin-film deposition

The epitaxial ferroelectric $PbTiO_3$ thin films investigated here were grown on (001)-oriented $KTaO_3$, MgO, and $SrTiO_3$ single-crystal substrates using the metalorganic chemical-vapor-deposition technique.[18] The deposition process was carried out in an inverted, vertical, warm-wall reactor with a resistively heated susceptor at a substrate temperature of 823 K. Typical growth rates ranged from 300 to 400 nm/h. Tetraethyl lead, $Pb(C_2H_5)_4$, and titanium isopropoxide, $Ti(OC_3H_7)_4$, were chosen as the metal precursors and argon as the carrier gas. A typical set of growth parameters for the deposition of $PbTiO_3$ on $KTaO_3(001)$ is as follows: the bubbler (containing the metal sources) temperatures were 22 and 14 °C for $Ti(OC_3H_7)_4$ and $Pb(C_2H_5)_4$, respectively, and the carrier-gas flow rates were respectively 1000 and 100 SCCM (where SCCM denotes cubic centimeters per minute at STP). Additional oxygen was used in the carrier-gas mixture to enhance the pyrolysis and to eliminate carbon incorporation. The oxygen flow rate was set at 8 SCCM, and the total reactor pressure was 75 Torr. Under the stated conditions, the partial pressures in the reactor, assuming full saturation of the metal sources, are calculated to be 8.9×10^{-3}, 1.4×10^{-3}, and 0.054 Torr, for $Ti(OC_3H_7)_4$, $Pb(C_2H_5)_4$, and oxygen, respectively. It is likely, however, that the carrier gas was not saturated with the metal precursors. Finally, the gas manifolds were heated about 20–40 °C above the highest source temperature to eliminate downstream condensation of the reactants.

B. Thin-film characterization techniques

A variety of techniques were used in characterizing the MOCVD-grown thin films including x-ray-diffraction methods for crystal-phase and orientation determination, scanning (SEM) and transmission electron microscopy (TEM) for the study of microstructure and surface morphology, high-resolution and Z-contrast[20] TEM for interfacial structures, energy-dispersive x-ray analysis (EDX), and Rutherford backscattering spectroscopy (RBS) for determining the thin-film composition and thickness, and ion channeling for studying crystallographic perfection. A Siemens digitized horizontal diffractometer with monochromated Cu $K\alpha$ radiation was used for the θ-2θ x-ray-diffraction scans at various temperatures, and a Nichrome-wire heater was used to heat the heterostructures in the diffractometer. In order to obtain an average of the integrated intensity of the x-ray peaks, the sample stage was rotated about the substrate-surface normal (along the angle ϕ) and rocked along the angle θ. (The angle χ represents the tilt angle of the substrate-surface normal out of the scattering plane.) For the determination of the in-plane epitaxial relationship and for the high-resolution θ-2θ scans, a 12-kW Cu $K\alpha$ rotating-anode generator with a vertically focusing LiF monochromator and a Huber four-circle diffractometer was employed in two different modes. High resolution was achieved using a Ge(111) analyzer crystal, and the low-resolution, high-count-rate experiments were carried out by placing a 2-mm slit about 20 cm from the sample. The 2θ positions and integrated intensities of the peaks were determined by curve fitting.

Thin-film-heterostructure samples were examined in cross-section and plan-view geometries by TEM. In both cases, the samples were first cut with a diamond saw to the desired geometry and crystallographic orientation and were then ion milled to a thickness of about 1000 Å. The interfacial structures including the domain structure and lattice-orientational relations were obtained using both high-resolution and Z contrast TEM. Plan-view TEM also provided a direct picture of the domain patterns.

The film composition and surface morphology were determined by energy-dispersive x-ray analysis and scanning electron microscopy, respectively, by employing a Hitachi 4000 SEM/EDX system. For the EDX measurements, standardless quantitative analysis that was calibrated with RBS was used. Rutherford backscattering experiments were performed that complemented the EDX results in addition to providing the calibration. Ion-channeling experiments were also performed along the [001] direction, and simulations of the RBS spectra were carried out using the RUMP program.[21]

III. CHARACTERIZATION OF THE HETEROSTRUCTURES

In the following subsections, the experimental results for the various heterostructures (including the three-dimensional epitaxial relationships, nature of the crystallinity, composition, and phases, and the defect and domain structures) will be presented.

A. $PbTiO_3/KTaO_3(001)$ system

Figure 1 shows a typical RBS spectrum for an epitaxial $PbTiO_3$ thin film deposited on a $KTaO_3(001)$ substrate. The dotted-dashed line in the figure represents

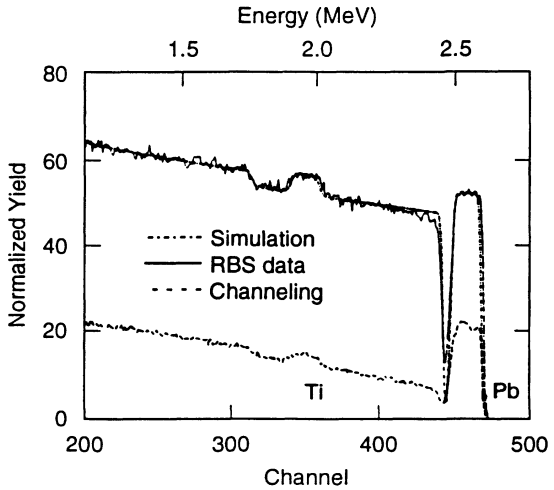

FIG. 1. RBS and ion-channeling spectra from $PbTiO_3$ films on (001) $KTaO_3$. The dotted-dashed line represents the simulation for $PbTiO_3$ while the dashed line indicates the axial channeling in the [001] direction.

the simulated RBS spectrum of stoichiometric $PbTiO_3/KTaO_3(001)$ as determined using the RUMP program,[21] while the solid line shows the experimental data. As can be seen, the simulation and experimental data are in good agreement, indicating that the film is composed of stoichiometric $PbTiO_3$ to within an uncertainty of about 5%. The thickness of the film is determined to be 150 nm, corresponding to a growth rate of 0.3 μm/h. Ion-channeling experiments were also performed on the sample along the [001] direction, and the results are shown by a dashed line in Fig. 1. Some channeling, with $\chi_{min}=40\%$, is observed for $PbTiO_3$ on $KTaO_3(001)$. This rather poor channeling efficiency for $PbTiO_3$ on $KTaO_3(001)$ can be attributed to the existence of a periodic domain-wall structure that will be discussed later.

Figure 2(a) shows a θ-2θ x-ray-diffraction pattern over a broad angular range for an epitaxial $PbTiO_3$ thin film deposited on $KTaO_3(001)$. As can be seen, the tetragonal film consists of both a and c domains. In the a and c domains, the c axis of the tetragonal unit cell is approximately parallel and perpendicular to the substrate surface, respectively. A rocking curve through the $PbTiO_3(300)$ peak showed a low mosaic spread with a full width at half maximum (FWHM) of about 0.3° as shown in Fig. 2(b). The exact nature of the epitaxial relationship (both out of plane and in plane) for both types of domains will be illustrated below.

Figure 3 shows a 360° ϕ scan around a small circle through the c-domain $PbTiO_3(002)$ reflections in which

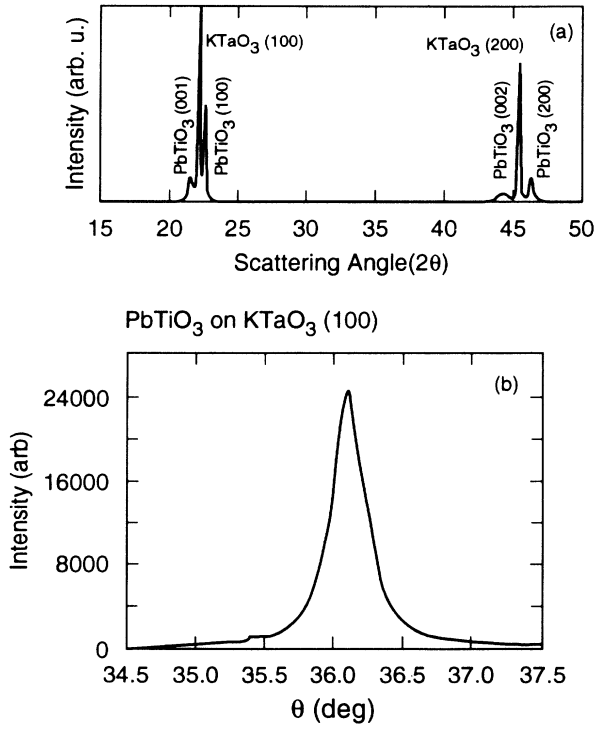

FIG. 2. (a) θ-2θ x-ray-diffraction pattern from a $PbTiO_3$ film on $KTaO_3(001)$ substrate. (b) Rocking curve of $PbTiO_3$ on $KTaO_3(001)$ showing the low mosaic spread in these films.

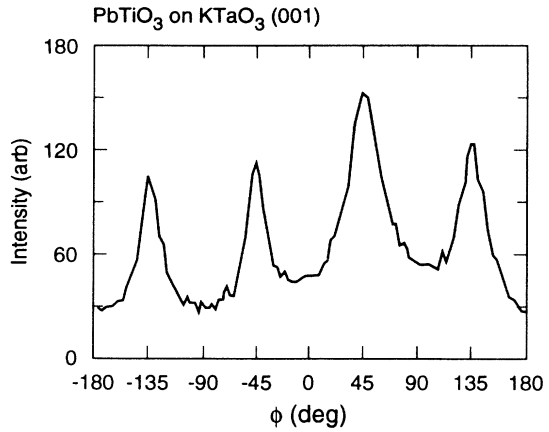

FIG. 3. 360° ϕ scan around a small circle through the $PbTiO_3(002)$ reflections of c domains. $\phi=0°$ is the in-plane $KTaO_3$ [110] direction.

$\phi=0°$ is the in-plane $KTaO_3$ [110] direction. Accounting for the substrate miscut direction (the surface normal was 2° from the $KTaO_3$ [001] direction and the in-plane projection of the surface normal was about 9° from the $KTaO_3$ [110] direction), c-domain $PbTiO_3(001)$ is found to be not exactly aligned with the $KTaO_3(001)$ surface. Instead, the c-domain $PbTiO_3(001)$ reflection is found to be split into four spots as seen in Fig. 3, each one tilted $\sim 1.5°$ away from the $KTaO_3$ [001] axis toward one of the four in-plane $KTaO_3$ [h00] axes. A similar ϕ scan from the a domains showed that the out-of-plane ($PbTiO_3$ [h00] and $KTaO_3$ [001]) axes of the film and the substrate are aligned.

A ϕ scan of the $PbTiO_3(220)$ reflection scattering from a domains is shown in Fig. 4, in which $\phi=0°$ is aligned with the in-plane $KTaO_3$ [100] direction. As can be seen, the $PbTiO_3\{220\}$ peaks are separated by about 90°, and there are no other peaks. This scan demonstrates the excellent in-plane epitaxial relationship between the film

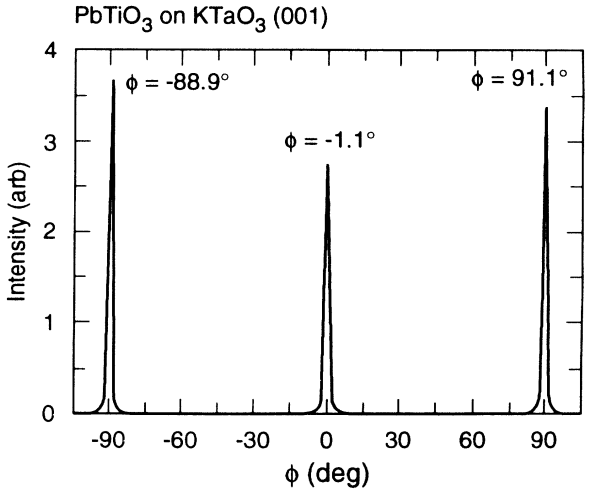

FIG. 4. ϕ-scan x-ray-diffraction pattern from the $PbTiO_3(220)$ reflection of the a domains showing the excellent in-plane epitaxial relations.

and substrate, indicating that the film is indeed three-dimensionally epitaxial. However, the in-plane orientation is such that the principal a and b axes of the film and substrate are *not* exactly aligned, as evidenced by the peak positions relative to in-plane $KTaO_3$ ⟨100⟩ directions. The actual epitaxial relationship is the alignment between the in-plane ⟨011⟩ directions of $PbTiO_3$ and the ⟨110⟩ directions of the substrate. A similar ϕ scan from the c domains showed that the in-plane ⟨100⟩ directions of the film and the substrate are aligned.

Analogous epitaxial relationships (of the a domains) and symmetry-breaking effects (discussed below) have recently been observed in c-axis-oriented orthorhombic $YBa_2Cu_3O_x$ thin films in which the domain preference was attributed to the rectangular basal plane of the c domain.[22] The apparent symmetry breaking in the population of possible domains in $YBa_2Cu_3O_x$ thin films has been attributed to the presence of small miscuts in the substrate surface toward the substrate $[hh0]$ direction. Moreover, it was proposed that the interfacial steps resulting from the miscut act as nucleation sites for twin boundaries. A similar mechanism is believed to be responsible for the symmetry breaking observed in the current heterostructure, since the a domains have a $(b \times c)$ rectangular basal plane, and the substrates exhibited similar miscuts ranging from 0.6° to 2°.

The evidence for this domain preference in the current heterostructure can be seen in Fig. 5. The plot shows the x-ray-diffraction intensity from $PbTiO_3(311)$ reflections of the a domains as the sample is rotated about the $KTaO_3(001)$ axis that has been aligned with the ϕ axis of the diffractometer. If the domain preference is not present, then a ϕ scan from a $PbTiO_3(h11)$ reflection of the a domains should consist of three peaks symmetrically placed around $\phi = \pm 45°$ with the center peak (at $\phi = \pm 45°$) having twice the intensity of the "side peaks."[22] As can be seen, this diffraction pattern is not representative of the case of four symmetry-equivalent domains. Rather, this is a situation in which only one of the two twinned pairs is present in the overlayer—resulting in a film with a single type of twin boundary. Consider, now, the peak splitting indicated in Fig. 5. Although it is smaller than the value that would be obtained using bulk lattice parameters, the calculated and experimentally determined values are nearly the same when the thin-film lattice parameters are used. The thin-film lattice parameters for this sample were determined to be $a = 3.924 \pm 0.0015$ Å, $b = 3.903 \pm 0.0015$ Å, and $c = 4.075 \pm 0.0020$ Å. From these values we determine the splitting to be 4.9°, while the experimental value is 4.7°. At this time, we do not have any direct observations of the interface to support the proposed symmetry-breaking mechanism or the orientational relationship between a surface ledge and the twin boundaries. It is, nevertheless, encouraging to see that this phenomenon appears to be common to both perovskite systems.

Figure 6 shows a high-resolution θ-2θ scan around the substrate (200) region for a 4500-Å-thick film on $KTaO_3$. Both of the observed $PbTiO_3$ Bragg peaks are clearly shifted from their expected bulk positions. In addition, the (002) peak (c domain) appears significantly broader than the (200) peak (a domain), implying that the correlation length is shorter for the c domains. Additional Bragg peaks located away from the substrate $(h00)$ axis were measured with the four-circle diffractometer and similarly were found to be shifted away from the expected bulk 2θ scattering angles (as seen above). The $PbTiO_3$ lattice parameters measured for a 4500-Å-thick film are as follows: in the c domain, $c = 4.095$ Å, and in the a domains, $a = 3.92$ Å, $b = 3.92$ Å, and $c = 4.08$ Å.

The observed shifts in the lattice parameters are in the expected direction when considering the effect of in-plane epitaxial lattice matching at room temperature. For example, the decrease in the c lattice parameter of the c domain can be explained as follows. The basal plane area $(a \times a)$ of the c domain is smaller than that of the substrate and would have to expand in order to match the substrate in epitaxial growth. This, in turn, would force the c lattice parameter to decrease through Poisson's ratio. A similar scenario would, accordingly, explain the increase in the a lattice pattern of the a domain. Howev-

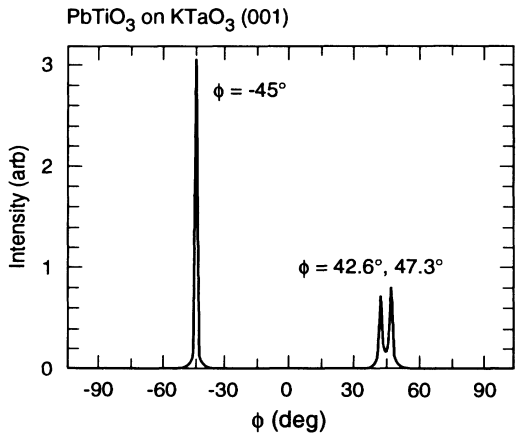

FIG. 5. ϕ-scan x-ray-diffraction patterns from $PbTiO_3(311)$ reflections of the a domains of $PbTiO_3$ on $KTaO_3(001)$ showing the in-plane epitaxial relationships. $\phi = 0°$ is the in-plane $KTaO_3$ [100] direction.

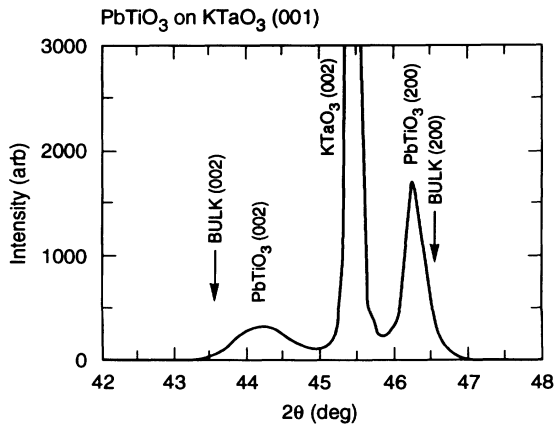

FIG. 6. High-resolution θ-2θ x-ray-diffraction pattern from a $PbTiO_3$ thin film on $KTaO_3(001)$ showing the peak shifts from the bulk values.

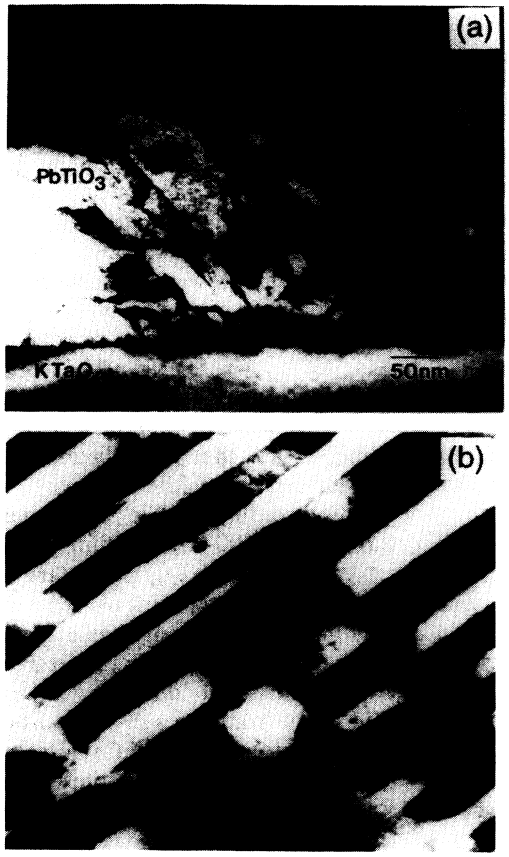

FIG. 7. TEM micrographs showing (a) the domain structure in cross section for a film with a thickness of 450 nm, and (b) the plan view of a film with a thickness of 25 nm. In (b), one can see the directionality of the domain patterns.

er, a decrease in the degree of tetragonality has been reported previously for MOCVD-grown $PbTiO_3$ films on fused silica and on Pt-coated alumina substrates.[23] In addition, we have measured lattice shifts in the same direction in a $PbTiO_3$ film on MgO, and it appears that lattice matching between the film and substrate is not the principal factor responsible for the observed deviation of the $PbTiO_3$ lattice parameters from the bulk values in these fairly thick films. Instead, we are proposing that these distortions are related to a minimization of the interfacial strain energy, which is introduced by differential thermal contraction and the ferroelectric phase transition of the $PbTiO_3$ layer on cooling from the deposition temperature. The resulting shifts in lattice parameter are functions of both the film thickness and temperature, and these effects will be discussed in more detail in a later section.

A transmission electron micrograph of $PbTiO_3/KTaO_3(001)$, as viewed in cross section and shown in Fig. 7(a), reveals a domain structure that consists of periodic a and c domains in an alternating sequence and separated by 90° domain walls[24] that form an angle of about 45° with the surface of the substrate. The domain widths are constant throughout the thickness of the film.

The domain structure shown in Fig. 7(a) represents only one of four symmetry-equivalent twinned islands if the substrate is miscut free. As discussed previously, and as indicated by the ϕ scans, often the films do not contain equal proportions of four twinned islands, but instead exhibit a strong preference for a particular pair. A TEM micrograph of a film whose thickness is 25 nm is shown in Fig. 7(b), and this micrograph demonstrates the strong preference for one twinning plane.

Figure 8 shows a Z-contrast TEM image for a $PbTiO_3$ thin film on $KTaO_3(001)$ with a film thickness of 150 nm, illustrating the interfacial structure and the alignment of atomic rows. Since this is a Z-contrast TEM, the white spots represent Ta and Pb for the substrate and film, respectively, while the black spots represent K and Ti. There are no misfit dislocations within the field of view, but one cannot rule out the possibility of the existence of

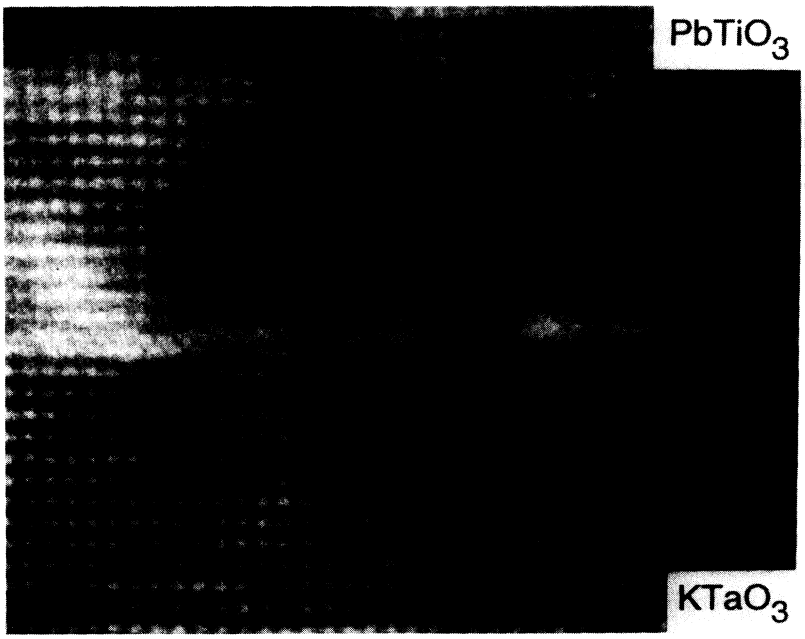

FIG. 8. High-resolution, Z-contrast TEM micrograph for a film with $t = 150$ nm. There are no misfit dislocations in the field of view.

misfit dislocations in thicker films.

Figure 9(a) shows the integrated x-ray-diffraction patterns obtained at various temperatures for a $PbTiO_3/KTaO_3(001)$ specimen. In the tetragonal structure below the Curie temperature T_c, there are three peaks, with the middle peak representing the substrate peak. The other two peaks are due to the a and c domains. In the cubic phase above T_c, all of the peaks merge into a single peak, and upon cooling, the tetragonal structure is recovered—indicating that the phase transition is reversible. The disappearance of the substrate peak after the initial heating might be due to a change in the alignment of the sample on the diffractometer due to the heating and cooling cycle. The high-temperature sample stage used to obtain these results did not have the capability for rotation about ϕ and rocking along θ, which is essential to keep the sharp reciprocal-lattice point of the substrate in the diffraction condition. This stage was necessary in order to observe the phase transition, however, because it was capable of reaching a temperature of 730 K. For measurements requiring better averaging for quantitative comparison purposes, a sample stage capable of rotation about ϕ and rocking along θ was employed. In Fig. 9(b), the tetragonal splitting between the (200) and (002) peaks is plotted as a function of temperature in order to illustrate the existence of the phase transition. Here, T_c is around 820 K for the $PbTiO_3$ film with thickness of 450 nm.

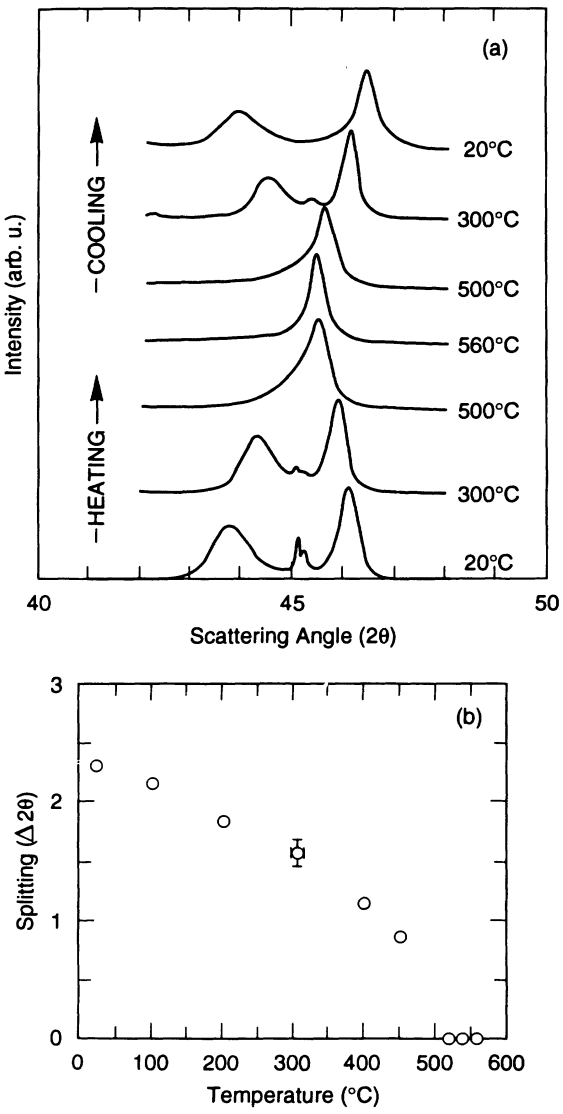

FIG. 9. (a) High-temperature x-ray-diffraction patterns showing the ferroelectric phase transition in $PbTiO_3$ on $KTaO_3(001)$ with a film thickness of 450 nm. (b) Plot of the splitting $[2\theta(200)\text{-}2\theta(002)]$ vs temperature showing the phase transition for the film.

B. $PbTiO_3$ on (001) $SrTiO_3$ system

Figure 10(a) shows a typical RBS spectrum for an epitaxial $PbTiO_3$ thin film deposited on (001) $SrTiO_3$. The dotted-dashed line represents the RUMP simulation for stoichiometric $PbTiO_3$ on a $SrTiO_3$ substrate. As can be seen, the simulation fits quite well to the experimental data, indicating that the film is stoichiometric $PbTiO_3$ to within an error of 5%. The thickness of this film was determined to be 135 nm, corresponding to a growth rate of 0.27 μm/h. Ion-channeling results in the [001] direction are shown by the dashed line in Fig. 10(a). A channeling yield χ_{min} of 29% is observed. For thinner films, however, the minimum yield was lower, e.g., 13% for a 47-nm-thick film. Improved channeling in these films, as

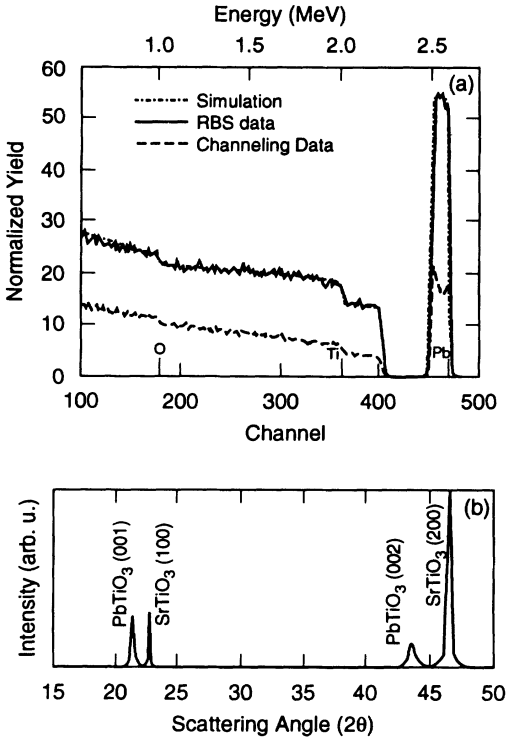

FIG. 10. (a) RBS and channeling spectra from an epitaxial $PbTiO_3$ film on $SrTiO_3(001)$. The dotted-dashed line represents the simulation of $PbTiO_3$ while the dashed line indicates the axial channeling in the [001] direction. The film thickness is 135 nm. (b) θ-2θ x-ray-diffraction pattern for $PbTiO_3$ on $SrTiO_3(001)$.

compared to that observed for the $PbTiO_3$ on $KTaO_3(001)$ case, can be attributed to the single-domain nature of the overlayer.

Figure 10(b) shows an x-ray-diffraction pattern (θ-2θ scan) over a broad angular range for a $PbTiO_3$ thin film deposited on (001) $SrTiO_3$. The presence of a domains in the $PbTiO_3$ film on (001) $SrTiO_3$ is not clear from the θ-2θ scan, due to an overlap between the a domain and the substrate peaks, but χ scans clearly indicate the absence of the a domains as will be described later. In addition, a θ scan (rocking curve) through the (002) reflection indicated that the epitaxy is good with a FWHM of about 0.6°. The film [001] axis is not tilted away from the substrate [001] axis—indicating that the alignment is with the substrate axis.

Figure 11 shows an x-ray ϕ scan through the $PbTiO_3\{202\}$ peaks of the c domains. As can be seen, the $\{202\}$ peaks are separated by 90° and are coincident with the in-plane $SrTiO_3$ $\langle 100 \rangle$ directions. This ϕ scan thus shows that the in-plane principal axes of the c domains and those of the substrate are aligned.

The absence of a domains in the overlayer can be verified by using a χ scan through the region of the reciprocal-lattice space where the (202) peaks from a and c domains should appear symmetrically about $\chi = 45°$. This situation for bulk $PbTiO_3$ has been illustrated in Fig. 12(a) while such a scan from a 135-nm-thick film is shown in Fig. 12(b). In Fig. 12(a), the solid lines represent the substrate [001] and [h00] directions while the dashed line represents the substrate [h01] direction. As can be seen in Fig. 12(b), only the peak from the c domains is present.

The absence of a domains can be explained on the basis of the excellent lattice matching between the $SrTiO_3$ lattice parameter and the in-plane $PbTiO_3$ a and b lattice parameters, as shown in Table I. The thin-film lattice parameters of the c domains of a film whose thickness is 135 nm are determined to be as follows: $a = b = 3.913 \pm 0.002$ Å and $c = 4.122 \pm 0.004$ Å. The shifts in lattice parameters with respect to the bulk values can be partly explained by the room-temperature lattice matching where

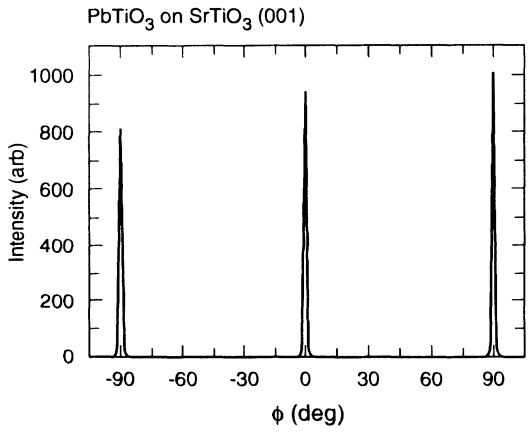

FIG. 11. ϕ-scan x-ray-diffraction pattern from a $PbTiO_3$ film on $SrTiO_3(001)$ showing the in-plane epitaxial relations. The reflection is from $PbTiO_3(202)$. $\phi = 0°$ is the in-plane $SrTiO_3$ [100] direction.

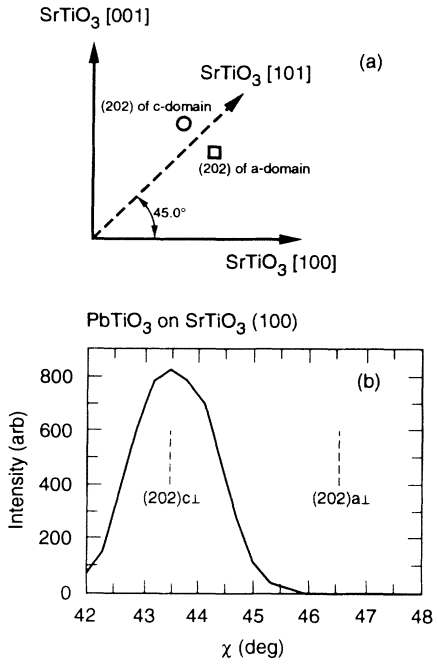

FIG. 12. (a) Schematic drawing of the reciprocal-lattice space perpendicular to the [0k0] direction for bulk $PbTiO_3$. (b) χ-scan x-ray-diffraction pattern of $PbTiO_3$ on $SrTiO_3(001)$ showing the absence of a and b domains.

the $a \times a$ of $PbTiO_3$ would expand in order to match the substrate. This, in turn, would contract the c axis through Poisson's ratio, resulting in an increase in a and a decrease in c. Thus, the excellent lattice matching between the two materials involved appears to dictate the formation of c domains as the heterostructure cools through the Curie temperature.

C. $PbTiO_3$ on the (001) MgO system

Figure 13(a) shows a typical RBS spectrum from an epitaxial $PbTiO_3$ thin film deposited on (001) MgO. In a manner similar to the other heterostructures, the simulation fits quite well with the experimental data, indicating that the film is stoichiometric $PbTiO_3$. The thickness of the film is determined to be 86 nm, corresponding to a growth rate of 0.35 μm/h. Ion-channeling experiments were also attempted on this and other samples along the [001] direction, but no channeling effects were observed. This observation might be partly attributed to the presence of a small polycrystalline phase in the film, whose x-ray-diffraction peaks would only be visible after expanding the intensity scale by several orders of magnitude.

Figure 13(b) shows a θ-2θ scan over a broad angular range along the substrate-surface normal of a $PbTiO_3$ thin film deposited on MgO(001). The scan provides evidence for the existence of both a and c domains. Using similar methods, the a and c axes (out of plane) in the respective domains are found to be aligned with the substrate [001] direction. The in-plane epitaxial relations were again determined from ϕ scans, and ϕ scans from a

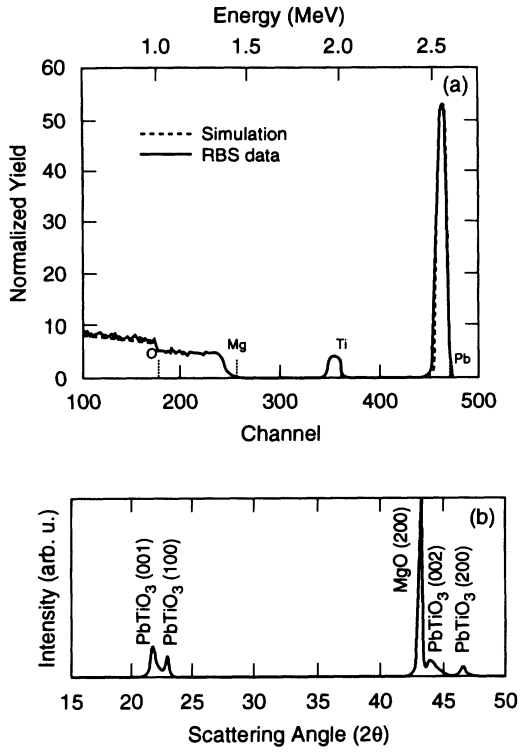

FIG. 13. (a) RBS spectrum from a $PbTiO_3$ film on MgO(001). The dashed line represents the simulation of $PbTiO_3$. (b) X-ray θ-2θ diffraction pattern from a $PbTiO_3$ film on MgO(001).

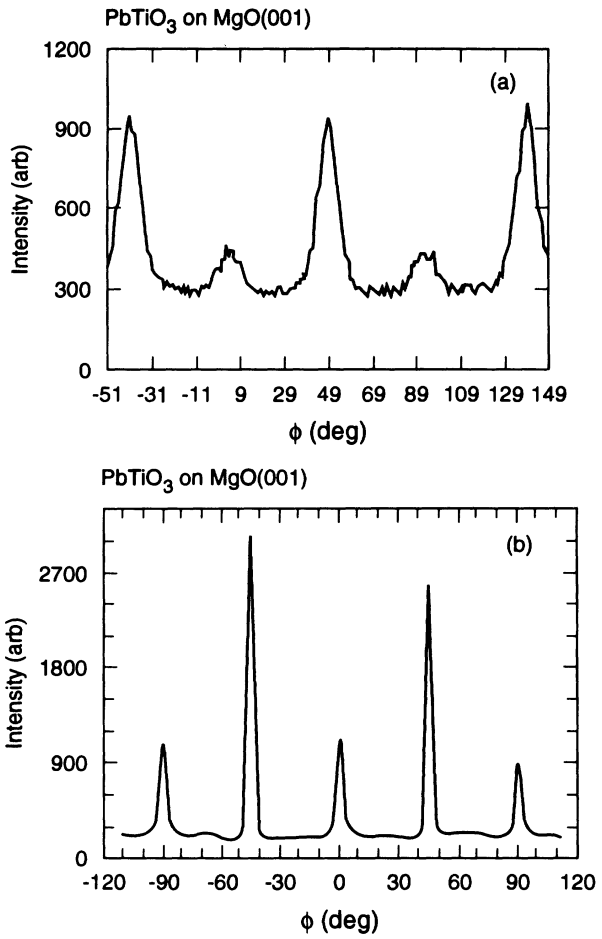

FIG. 14. (a) ϕ scan from a domains in $PbTiO_3$ on MgO(001) showing different types of island arrangements. $\phi=49°$ is the in-plane MgO [100] direction. The film thickness was 150 nm. (b) ϕ scan from c domains in $PbTiO_3$ on MgO(001) showing different types of c domains. The film thickness was 86 nm. $\phi=0°$ is the in-plane MgO [100] direction.

(202) reflection for a and c domains are shown respectively in Figs. 14(a) and 14(b). Note that in Fig. 14(a) $\phi=49°$ refers to the in-plane MgO [100] direction whereas in Fig. 14(b), $\phi=0°$ refers to the in-plane MgO [100] direction. These figures indicate that there are two types of both a and c domains: one (type I) having the in-plane alignment between [100] axes of the film and the substrate [peaks at $\phi=139°$ and $-41°$ in Fig. 14(a), and peaks at $\phi=0°$ and $\pm 90°$ in Fig. 14(b)], while in the other (type II), the [100] direction of the film forms an angle of 45° with the [100] direction of the substrate (remaining peaks in each figure).

The two types of domains observed here can be explained by considering possible "coincidence superlattices" (also known as the near-coincidence lattice-site model) for the heterostructure. Figure 15 shows the arrangements for the type II of the c domains determined based on a rigid model in which elastic deformation is not allowed for both the film and the substrate. As can be seen, a $(3a \times 3a)$ superlattice of $PbTiO_3$ coincides with a diagonal $[2\sqrt{2}(a \times a)]$ superlattice of MgO. For the a domains, the coincidence superlattice would be between $(3b \times 3c)$ of $PbTiO_3$ and a diagonal $[2\sqrt{2}(a \times a)]$ of MgO. Although an elaborate coincidence superlattice can be devised for type I, the 1×1 cell appears to be the most meaningful physically since the misfits are about 7.5 and 1.5% respectively for a and c lattice parameters. The rotated islands (type II) appear to be the more abundant of the two in c domains, whereas in a domains they are less abundant. For a film with a thickness of 150 nm,

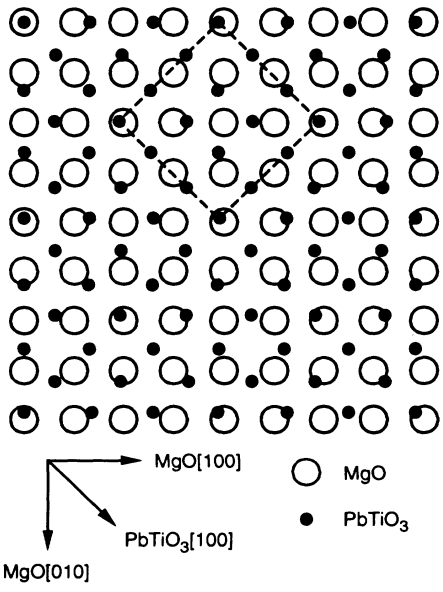

FIG. 15. Coincidence superlattice of type II for the c domains in $PbTiO_3$ on MgO(001). The dashed square shows the unit cell for the type-II superlattice.

however, the relative abundance of the type-I and the type-II domains reverses for both a and c domains. Because of the complex domain structures observed on MgO, it is not surprising that the FWHM's of the rocking curves for these films are greater than those obtained for $PbTiO_3$ on $KTaO_3$ and $PbTiO_3$ on $SrTiO_3$ at about 2°.

IV. THEORETICAL MODELING

The theoretical model used to explain the observed domain-formation phenomena in the case of $PbTiO_3$ films on $KTaO_3(001)$ will be described in the following subsection and, in particular, thickness- and temperature-dependence relationships will be analyzed.

Total energy of a heterostructure

As described above, the thin films assume a heterogeneous domain structure with periodically alternating domains whose widths are constant throughout the film thickness [see Fig. 7(a)]. The domain structure within one of the four variants of the twinned islands has already been presented in Ref. 14. In order to quantify the strain relaxation due to domain formation, one must first determine the total-energy functional of the heterostructure by considering the various energy contributions. This has been accomplished by using linear-elasticity theory and a Landau-Ginzburg-Devonshire (LGD) type of phenomenological theory for the substrate and overlayer, respectively, and then minimizing the total energy with respect to various independent variables by taking into account the epitaxial-strain constraints.

Three separate contributions to the total energy are considered:

$$E_t = E_s + E_d + E_f \ , \tag{1}$$

where E_s is the elastic energy stored in the substrate in the vicinity of the interface, E_d is the domain-wall-creation energy obtained from the LGD free energy, and E_f is the LGD free energy of the film which depends on the polarization and spontaneous strain.[25,26] The spontaneous strain in the films is defined with respect to the extrapolated lattice parameter a_c of cubic lead titanate [i.e., $x_i=(a_i-a_c)/a_c$], while epitaxial misfits are defined with respect to the lattice parameter a_s of the substrate [i.e., $\varepsilon_i=(a_i-a_s)/a_s$]. E_s will be considered first. E_f and E_d will be considered subsequently.

The a and c domains are assumed to be locally coherent with the substrate at the interface. Based on the schematic diagram of the observed domain structure, the strain-distribution function $\varepsilon(x,0)$ imposed on the substrate at the interface is modeled as a periodic step function as shown in Ref. 14. Due to the periodic nature of $\varepsilon(x,0)$, it can be expressed as

$$\varepsilon(x,0)=\varepsilon(u+nl,0)$$

where $l=l_a+l_c$ with $0<u<l$, and n is an integer. Here, l is the domain period consisting of one a and an adjacent c domain. Expansion into a Fourier series yields the following result:

$$\varepsilon(x,0)=\sum_n \left[A_n \cos\frac{2\pi n x}{l} + B_n \sin\frac{2\pi n x}{l} \right] , \tag{2}$$

where

$$A_n = \frac{1}{\pi n}(\varepsilon_a+\varepsilon_c)\sin 2\pi n w \ ,$$

and

$$B_n = \frac{1}{\pi n}(\varepsilon_a+\varepsilon_c)(1-\cos 2\pi n w) \ .$$

In Eq. (2), w is defined to be the fraction of the a domains, and thus $l_a=lw$ and $l_c=(1-w)l$; ε_a and ε_c are the misfits at the interfaces of c and a domains, respectively.

The average strain energy per unit area of the interface of that part of the substrate which extends from the interface out to a distance t from it is given by[27]

$$E(t)=\frac{1}{l}\int_0^t dz \int_0^l dx \left[\frac{1}{4\mu} \right] [(1-\nu)(\sigma_{xx}^2+\sigma_{zz}^2) - 2\nu\sigma_{xx}\sigma_{zz}+2\sigma_{zx}^2] \ , \tag{3}$$

where σ_{ij} denote components of the stress tensor, and μ and ν are the shear modulus and Poisson's ratio of the substrate, respectively. Now, following an approach similar to that taken by van der Merwe and Ball[27] and Timoshenko,[28] where the stress function ϕ is determined first, the stress function must satisfy the Airy stress equation

$$\nabla^4\phi=0 \ , \tag{4}$$

with the stresses defined by

$$\sigma_{xx}=\frac{\partial^2\phi}{\partial z^2}, \quad \sigma_{zz}=\frac{\partial^2\phi}{\partial x^2}, \quad \text{and} \quad \sigma_{zx}=-\frac{\partial^2\phi}{\partial x\,\partial z} \ . \tag{5}$$

The desired solution of the stress function should be such that (1) the strain has the boundary value $\varepsilon(x,0)$ of Eq. (2) at $z=0$, and (2) the stresses vanish at the free boundary $z=+\infty$. Note that interface is taken as $z=0$ and that the positive z direction is taken as going into the substrate. From the periodicity of the domain pattern, one expects the stress to have the same periodicity l. In applying the boundary condition (2), the following expression is used to relate the strain and stress:

$$\varepsilon_{xx}(x,0)=\varepsilon(x,0)=\frac{(1-\nu)}{2\mu}\sigma_{xx}(x,0) \ . \tag{6}$$

Thus, we obtain the following form of ϕ:

$$\phi(x,z)=Rz\sum_{n=1} M_n(x)\exp(-G_n z) \ , \tag{7}$$

where

$$R=-\frac{\mu l}{2\pi(1-\nu)}, \quad M_n(x)=\frac{A_n}{n}\cos G_n x+\frac{B_n}{n}\sin G_n x \ ,$$

and

$$G_n=\frac{2\pi n}{l} \ .$$

Carrying out the integration in Eq. (3) by using the stresses calculated from Eqs. (5) and (7) one obtains the result

$$E(t)=\frac{\mu(\varepsilon_a+\varepsilon_c)^2 l}{4\pi^3(1-\nu)^2}\sum_{n=1}^{\infty}\frac{\sin^2\pi n w}{n^3}Q_n(t)\ , \tag{8}$$

where

$$Q_n(t)=\{(1+\nu)+[-2\nu G_n^2 t^2+(4-6\nu)G_n t-(1+\nu)]\times\exp(-2G_n t)\}\ .$$

In the limit $t\rightarrow\infty$,

$$E(t\rightarrow\infty)=\frac{\mu(1+\nu)\alpha(w)}{4\pi^3(1-\nu)^2}(\varepsilon_a+\varepsilon_c)^2 l\ , \tag{9}$$

where

$$\alpha(w)=\sum_{n=1}^{\infty}\frac{\sin^2\pi n w}{n^3}\ .$$

Equation (9) has the same form as that given by Roitburd[12] and by Khachaturyan[29] for twin bands in martensites.

The strain energy stored in the substrate will have the form given in Eq. (9) with the misfit terms defined with respect to the substrate lattice parameter. Thus,

$$E_s=\frac{\mu(1+\nu)\alpha(w)}{8\pi^3(1-\nu)^2}[(\varepsilon_a+\varepsilon_c)^2+(\varepsilon_b+\varepsilon_c)^2]lL_1L_2\ . \tag{10}$$

Note that we have differentiated between a and b domains in the above equation. Let us assume that N_a, N_b, and N_c show the domain populations for a, b, and c domains, respectively. We assume that $N_a=N_b$ and $\varepsilon_a=\varepsilon_b$ for the actual calculations because of the symmetry, and L_1 and L_2 are the dimensions of the film along the x and y axes, respectively.

For numerical convenience, $\alpha(w)$ was approximated with

$$\alpha(w)\approx\alpha(N_c)=\frac{39.5N_c^3}{[\exp(7.8N_c^2)-0.999]}\ , \tag{11}$$

where

$$w=\frac{(1-N_c)}{(1+N_c)}\ ,$$

and the values given in Table II were used for the material constants.

The creation energy of a 90°-domain wall in $PbTiO_3$ can be calculated by following a LGD-type theory used previously by Bulaevskii.[33] The domain-wall energy e_d per unit area for a 90°-domain wall (following Bulaevskii's notation) is

$$e_d=\frac{\kappa P^2}{\delta}(1+\alpha^2)I(\alpha)\ , \tag{12}$$

where

$$I(\alpha)=\int_{-\infty}^{\infty}\frac{\cosh^2 t\,dt}{(\alpha+\cosh^2 t)^3}\ ,$$

$$\alpha=\frac{c_1}{2c_1+3b_1/2},\ \text{and}\ \delta=\left[\frac{\kappa}{A_1(c_1+b_1/2)}\right]^{1/2}\ .$$

By substituting the expressions

$$c_1=\frac{C_1P^4}{4A_1}\ \text{and}\ b_1=\frac{B_1P^2}{4A_1}\ ,$$

α and δ can be expressed as

$$\alpha=\frac{1}{[2+3B_1/C_1P^2]}\ \text{and}\ \delta=\frac{2}{P^2}\left[\frac{\kappa}{(C_1P^2+B_1)}\right]^{1/2}\ . \tag{13}$$

In Eq. (12), κ is the coefficient in the spatial-gradient term of the LGD free energy, B_1 and C_1 are terms defined by the compliances used in a thermodynamic free energy for a cubic ferroelectric crystal from Ref. 33, and δ is the domain-wall width for a 90°-domain wall. Thus, the total-energy contribution by the domain walls is equal to $e_d(L_2L_3)(L_1/l)$. We calculate e_d to be 0.24 J/m^2 for $PbTiO_3$ at 23 °C by using a polarization value of $P=0.75$ C/m^2.[31]

The energy density of the ferroelectric $PbTiO_3$ layer can be expressed, in general, as[5,25,26]

TABLE II. A list of elastic constants of $PbTiO_3$, $KTaO_3$, MgO, and $SrTiO_3$. All terms except ν have been divided by a factor of 10^{11} N/m^2.

Constants	$PbTiO_3$[a]	$KTaO_3$[b]	$SrTiO_3$[c]	MgO[c]
c_{11}	1.433	4.31	3.156	
c_{12}	0.322	1.30	1.027	
c_{13}	0.241		1.215	
c_{33}	1.316			
c_{44}	0.558			
c_{66}	0.556			
Y	1.34	3.71	2.43	3.105
μ	0.58	1.51	1.06	1.332
ν	0.16	0.23	0.25	0.166

[a]Reference 32.
[b]Reference 31.
[c]Reference 30.

$$e_f(P,x_{ik})=\tfrac{1}{2}\chi^x P^2+\tfrac{1}{4}\xi_{11}^x P^4+\tfrac{1}{6}\xi_{111}^x P^6+\tfrac{1}{2}c_{11}(x_{11}^2+x_{22}^2+x_{33}^2)+c_{12}(x_{11}x_{22}+x_{11}x_{33}+x_{22}x_{33})+c_{44}(x_{12}^2+x_{13}^2+x_{23}^2)+q_{11}x_{33}P^2+q_{12}(x_{11}+x_{22})P^2\ , \tag{14}$$

where P and x_{ik} are the spontaneous polarization and the strain-tensor components, χ^x, ξ^x_{ij}, and ζ^x_{ijk} are the dielectric stiffness and the higher-order stiffness coefficients at constant strain, and c_{ij} and q_{ij} are the elastic compliance and the cubic-electrostrictive constants, respectively.

Since the strain involved is of the planar type (i.e., no shearing deformations), any component of the strain tensor with $i \neq j$ would be zero. By applying the relationships $x_{ik}=0$ for $i \neq k$ and $x_{ii}=x_i$, one arrives at the following equation:

$$\begin{aligned} e_f(P,x_{ik}) = & \tfrac{1}{2}\chi^x P^2 + \tfrac{1}{4}\xi^x_{11}P^4 + \tfrac{1}{6}\xi^x_{111}P^6 \\ & + \tfrac{1}{2}c_{11}(x_1^2+x_2^2+x_3^2) \\ & + c_{12}(x_1x_2+x_1x_3+x_2x_3) \\ & + q_{11}x_3P^2 + q_{12}(x_1+x_2)P^2 \ . \end{aligned} \tag{15}$$

The total-energy contribution from the film is, thus, $E_f = e_f L_1 L_2 L_3$. The constants used for $PbTiO_3$ were compiled from published bulk $PbTiO_3$ results.[25,26,31,32] The elastic constants c_{ij} are listed in Table II. The derivation of the various constants used in Eqs. (12) and (15) has been outlined in Ref. 34, and the various notations used by different authors are listed.

In the minimization process, an elastic Gibbs free energy $G_1(P,X_i)$ was first formulated which has a functional dependence on the stress rather than on the spontaneous strains. The elastic Gibbs energy has the same form as in Eq. (15) with replacements of x_i by X_i and by the appropriate compliances as follows,[25,26]

$$\begin{aligned} G_1(P,X_i) = & \alpha_1 P^2 + \alpha_{11}P^4 + \alpha_{111}P^6 + \tfrac{1}{2}s_{11}(X_1^2+X_2^2+X_3^2) \\ & + s_{12}(X_1X_2+X_1X_3+X_2X_3) + Q_{11}X_3P^2 \\ & + Q_{12}(X_1+X_2)P^2 \ , \end{aligned} \tag{16}$$

where α_1, α_{11}, and α_{111} are the dielectric stiffness and the higher-order stiffness coefficients at constant stress, and s_{ij} and Q_{ij} are the elastic compliance and the electrostrictive constants, respectively. Through a Legendre transformation, Eq. (16) was converted into the Helmholtz free energy expressed in terms of the spontaneous strains. This approach was used since the most reliable data are available for the constants of Eq. (16).[25,26] The Legendre transformation could be easily performed by using MATHEMATICA,[35] a computer program that is capable of symbolic manipulations.

The total-energy function obtained by combining all three contributions noted above has dependences on five parameters. These are the spontaneous polarization, spontaneous strain (three parameters), and domain period. By minimizing this total energy at a given film thickness and temperature, one can determine these five parameters which, in turn, can be used to determine other related properties such as the relative domain population N_c. A minimization routine based on the Marquardt algorithm in MATHEMATICA[35] was used for this purpose.

An expression for N_c, the normalized relative population of the c domains, can be derived from the coherency condition that the lattice parameters of the film and the substrate must be equal at the interface. This results in the following equation for a situation in which a fully relaxed overlayer at the growth temperature is assumed:

$$\int_{T_s}^{T_0} \alpha_s(T)dT = \int_{T_s}^{T_c} \alpha_f(T)dT + N_c\varepsilon_a + N_a\varepsilon_c + N_b\varepsilon_b \ , \tag{17}$$

where T_s = growth temperature, T_c = phase transition temperature, and T_0 = measurement temperature. By assuming $N_a = N_b$ and $N_a + N_b + N_c = 1$, one obtains the expression for N_c in terms of ε_i, which can be expressed in terms of the spontaneous strains x_i. Thus, by using the x_i obtained through the minimization of the total energy, one can determine the relative population of the domains. For the case of unrelaxed epitaxial-misfit strain at the growth temperature, an additional term, $\Delta\varepsilon_G = \{[a_c(T_s) - a_s(T_s)]/a_s(T_s)\}$, was added to the left-hand side of Eq. (17).

Investigating the temperature dependence at a given thickness, the only additional factor that must be taken into account is the lattice-parameter change due to temperature for both the film and the substrate. Various compliances which appear in the LGD free energy were taken to be independent of temperature, except for the Curie-Weiss term χ in Eq. (14).[36]

V. COMPARISON BETWEEN EXPERIMENT AND THEORY

The predictions of the theoretical model and the experimental data for the various heterostructures are compared in the following subsections, considering first the thickness dependence of the relative domain population and the spontaneous strains, and subsequently the temperature dependence of these parameters.

A. $PbTiO_3$ on $KTaO_3$(001) system

The calculated and experimentally determined (as measured by using the integrated x-ray intensities from θ-2θ scans) relative c-domain populations as a function of the film thickness L_3 have been presented in our previous publication.[14] These results indicate that, depending on the film thickness, the film grows either in its coherent pseudomorphic cubic phase, retaining its epitaxial strain, or in a fully relaxed cubic phase with no epitaxial strain; both of which form a periodic domain pattern as they cool through the Curie temperature. For film thicknesses less than about 34 nm, the equilibrium structure consists only of a domains and equivalent b domains. From about 34 to 250 nm, the films appear to grow without relieving the epitaxial-misfit strain, leading to alternating a and c domains having the thickness dependence shown in Ref. 14. For film thicknesses greater than about 250 nm, the film appears to be almost fully relaxed at the growth temperature, presumably as a result of misfit-dislocation formation. Therefore, a thickness of 250 nm can be considered as the critical thickness at the growth temperature for this film.

The experimental and calculated spontaneous strains x_3 and x_1 as a function of the film thickness were also shown in Ref. 14. The spontaneous strains are deter-

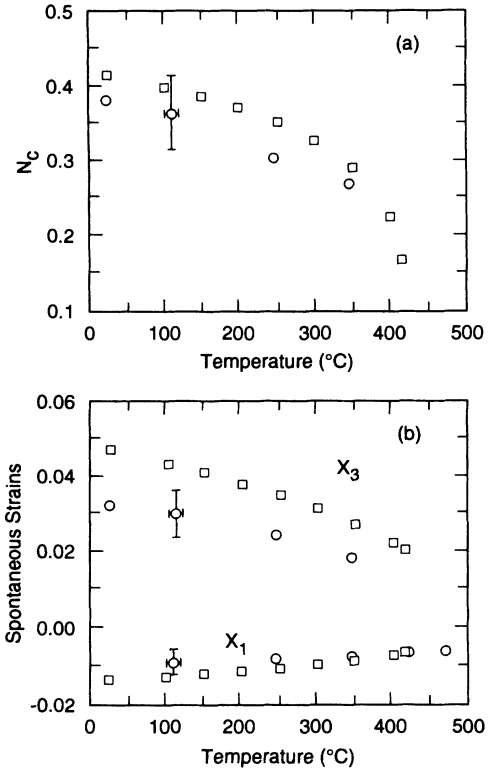

FIG. 16. Temperature dependence of (a) the relative domain population N_c and (b) spontaneous strains x_i for a film thickness of about 250 nm. The heterostructure is $PbTiO_3$ on $KTaO_3(001)$. The circles and squares are the experimental and predicted values, respectively.

mined by using the 2θ positions from θ-2θ x-ray-diffraction scans. There was a reasonably good agreement for both x_3 and x_1, supporting the validity of the present model. The spontaneous strains approach the bulk values for thicker films as one would expect. This implies that the domain formation considered above does not fully relax the film.

Figure 16(a) shows a plot of N_c as a function of the sample temperature for a film with a thickness of approximately 250 nm. The circles and squares are the experimental and predicted values, respectively. Here, N_c could be determined only up to 350 °C because of the overlap between the (001) peak of the film and the (001) peak of the substrate at higher temperatures. One can see, however, that there is reasonable agreement between the model predictions and the experimental observations. Figure 16(b) shows the experimental and calculated spontaneous strains as a function of sample temperature, and, again, one can see that there is reasonable agreement verifying the utility of this approach. Below, we present the experimental results without the theoretical predictions, because of the complexity of the systems.

B. $PbTiO_3$ on $SrTiO_3(001)$ system: Temperature dependence of x_3

Because of the overlap between the (001) peaks of the substrate and the film in cases where *a* domains may exist, x_1 and N_c could not be determined for this system.

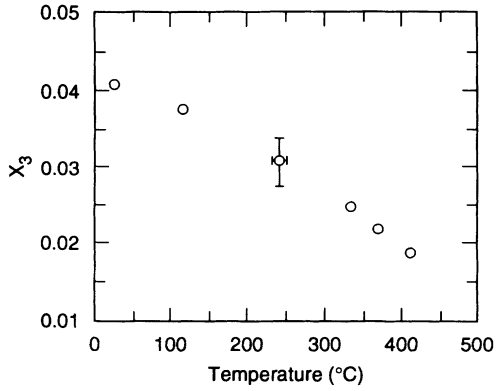

FIG. 17. Measured spontaneous strain x_3 plotted as a function of the sample temperature for $PbTiO_3$ on $SrTiO_3(001)$.

Therefore, only the temperature dependence of the measured spontaneous strain x_3 is shown in Fig. 17 for a film with a thickness of 135 nm. As expected, the spontaneous strain decreases as a function of temperature. A determination of the strain near the transition temperature is difficult due to the merging of the diffraction peaks.

C. $PbTiO_3$ on MgO(001) system

Figure 18(a) shows a plot of the measured relative domain population N_c as a function of the film thickness, and N_c clearly decreases as the film thickness increases, finally reaching a constant value of ≈ 0.75. The existence of a complex domain structure in $PbTiO_3$ thin films

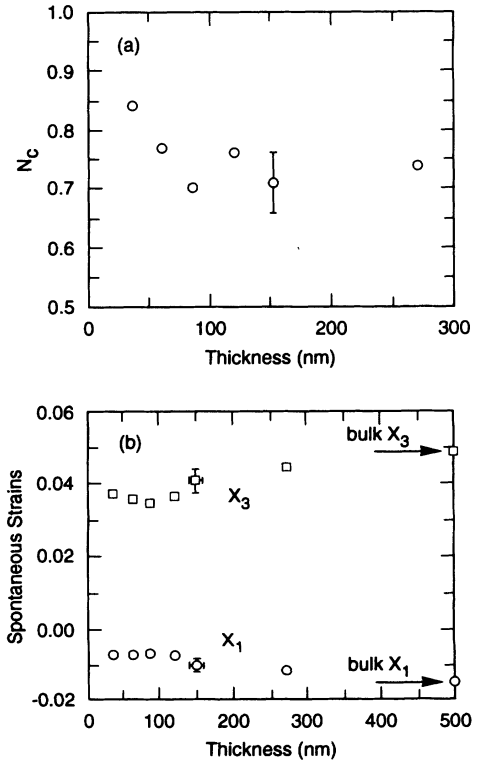

FIG. 18. Plot of the experimentally determined (a) abundance of the *c* domains N_c and (b) spontaneous strains as a function of the film thickness for $PbTiO_3$ on MgO(001).

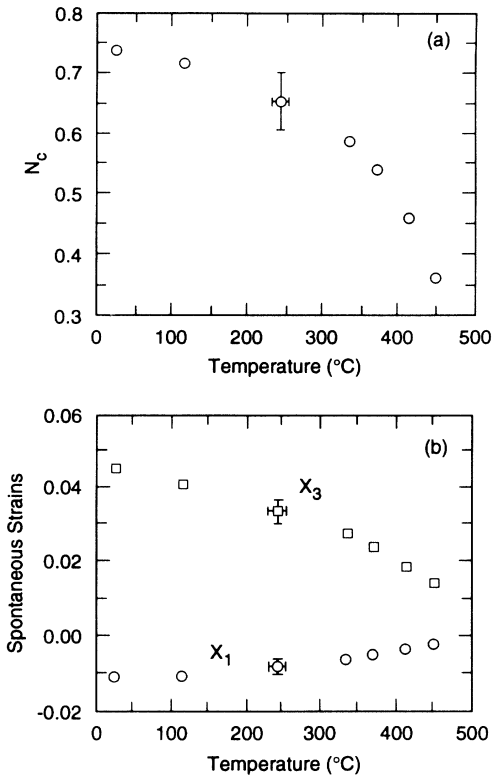

FIG. 19. Plot of the experimentally determined (a) N_c and (b) spontaneous strains as a function of the sample temperature for $PbTiO_3$ on MgO(001). The thickness of the film is 280 nm.

grown on (001) MgO involving different types of coincident superlattices does not permit a tractable theoretical modeling of this system.

The thickness dependence of the measured spontaneous strains is shown in Fig. 18(b). As expected, they approach the bulk values as the thickness increases. With decreasing thickness, there appears to be a decrease in x_3 and an increase in x_1 around 100 nm, and this anomaly appears to be a real effect. The detailed elucidation of this behavior, however, would require more detailed TEM and x-ray-diffraction studies.

Figures 19(a) and 19(b) show the measured temperature dependences of N_c and the spontaneous strains, respectively, for a 280-nm-thick film. Both N_c and the spontaneous strains qualitatively follow the same trend observed in the other heterostructures, i.e., $PbTiO_3$ on $KTaO_3$ and $SrTiO_3$, and, again, an elucidation of the effects of epitaxial-misfit strain would require in-depth TEM and x-ray characterization.

VI. CONCLUSIONS

The MOCVD growth of a simple perovskite, namely, ferroelectric lead titanate ($PbTiO_3$) has been achieved in the form of three-dimensional, epitaxial thin films on various single-crystal substrates, and these epitaxial heterostructures have been analyzed in some detail. The heterostructures considered are $PbTiO_3$ on the (001) surfaces of potassium tantalate ($KTaO_3$), magnesium oxide (MgO), and strontium titanate ($SrTiO_3$). It was found that the presence of the ferroelectric phase transition in $PbTiO_3$ leads to a unique strain-accommodating mechanism, in which domain patterns form (as the system cools through the Curie temperature) to limit the extension of interfacial strain in the heterostructure, and thus minimize the total energy of the heterostructure. It was also found that these domain patterns depend very strongly on both the film thickness and sample temperature.

The strain-accommodating mechanisms in these heterostructures depended on both the lattice and thermal-expansion-coefficient mismatch between the film and the substrate. In the $PbTiO_3$ on $KTaO_3(001)$ system, interfacial strain was accommodated by the formation of periodic domain patterns in the overlayers. For $PbTiO_3$ on $SrTiO_3(001)$, a system that exhibits excellent lattice match between the a lattice parameters of the film and the substrate, the film existed as a single c domain. The $PbTiO_3$ on MgO(001) system, with a poor lattice match for both a and c axes, appeared to seek the energy minimum by locking into domains of two-dimensional near-coincidence superlattices.

The a- and c-domain structure of the overlayer was also found to be influenced by miscuts in the substrate. In the $PbTiO_3$ on $KTaO_3(001)$ system, only two of the possible four symmetry-equivalent twinned islands were found in the overlayer, and the observed symmetry breaking was attributed to a specific miscut in the substrate surface.

A theoretical analysis of the domain-pattern formation has been performed by using linear-elasticity and a Landau-Ginzburg-Devonshire-type phenomenological theory for the substrate and overlayer, respectively. It was found that on $KTaO_3$ the film grows either in a pseudomorphic cubic phase (below about 250 nm) retaining the epitaxial-misfit strain at the deposition temperature or in a fully relaxed cubic phase at the growth temperature. It was also found that the domain pattern consisted entirely of a and b domains below a certain thickness. The theoretical predictions and the experimental measurements for $PbTiO_3$ on $KTaO_3(001)$ show good agreement in both the thickness and temperature dependence of the relative domain populations and the spontaneous strains. Although many of the results obtained here can be directly applied to other similar oxide heterostructures, such as high-T_c superconductors with layered perovskite structures, additional work is needed to elucidate further the nature of the epitaxial phenomena observed for $PbTiO_3$ on MgO(001).

The theoretical model developed in the course of this investigation yielded promising results in predicting the behavior of $PbTiO_3$ heterostructures; however, there are aspects of the model which can be improved further. For example, questions dealing with the energy contribution from the domain wall can be raised, and it appears that a correlation to the theory of Bulaevskii has been made recently by Cao and Cross,[37] which could be considered. An additional aspect deals with the apparent twinning associated with the a domains. In the present model, only one of four possible "twinned islands" which consisted of alternating a and c domains was examined; however, as evidenced by the ϕ scan of Fig. 4, there are two of these twinned islands and an associated twinning plane; i.e., the

twinning within the *a* domain into *a* and *b* domains. Thus, the total-energy term can be correlated by an energy term (energy cost) associated with the creation of this twinning plane. Both of these factors may further enhance the accuracy and generality of the model. Finally, a more fundamental aspect deals with the usage of the constants (both elastic constants and various LGD free-energy-related compliances) for ferroelectric $PbTiO_3$ in the model calculations. In light of the existence of surface layers with nonbulklike ferroelectric properties,[38] the use of bulk values for the thin-film energy contribution may introduce significant errors (although these values are the only ones available at the present time). To resolve this issue, one can consider an investigation of free-standing thin films to determine the behavior of these materials as a function of film thickness and temperature, and these values can then be incorporated into the present theoretical model.

ACKNOWLEDGMENTS

The authors would like to acknowledge A. Zangwill for helpful discussions and a critical reading of the manuscript. This work was partially supported by the Division of Materials Sciences, U.S. Department of Energy under Contract No. DE-AC05-84OR21400 with Martin Marietta Energy Systems, Inc.

*Present address: Solid State Division, Oak Ridge National Laboratory, Oak Ridge, TN 37831.

†Author to whom all correspondence should be addressed.

‡Present address: Center for Solid State Science, Arizona State University, Tempe, AZ 85287.

[1] *Epitaxy of Semiconductor Layered Structures,* edited by R. T. Tung, L. R. Dawson, and R. L. Gunshor, MRS Symposia Proceedings No. 102 (Materials Research Society, Pittsburgh, 1988).

[2] T. Sands, C. J. Palmstrom, J. P. Harbison, V. G. Keramidas, N. Tabatabaie, T. L. Cheeks, R. Ramesh, and Y. Silberberg, Mater. Sci. Rep. **5**, 99 (1990).

[3] M. K. Wu, L. R. Ashburn, C. J. Torng, P. H. Hor, R. L. Meng, L. Gao, Z. J. Huang, Y. Q. Wang, and C. W. Chu, Phys. Rev. Lett. **58**, 908 (1987).

[4] Z. Z. Sheng and A. M. Hermann, Nature **332**, 138 (1988).

[5] M. E. Lines and A. M. Glass, *Principles and Applications of Ferroelectrics and Related Materials* (Clarendon, Oxford, 1977).

[6] V. G. Gavrilyachenko, R. I. Spinko, M. A. Martynenko, and E. G. Fesenko, Fiz. Tverd. Tela (Leningrad) **12**, 1532 (1970) [Sov. Phys. Solid State **12**, 1203 (1970)].

[7] K. Iijima, Y. Tomita, R. Takayama, and I. Ueda, J. Appl. Phys. **60**, 361 (1986).

[8] M. H. Francombe and S. V. Krishnaswamy, J. Vac. Sci. Technol. A **8**, 1382 (1990).

[9] R. Bruinsma and A. Zangwill, J. Phys. (Paris) **47**, 2055 (1986).

[10] C. A. Ball and J. H. van der Merwe, in *Dislocations in Solids,* edited by F. R. N. Nabarro (North-Holland, Amsterdam, 1983), Chap. 27.

[11] J. W. Matthews and A. E. Blakeslee, J. Cryst. Growth **27**, 118 (1974).

[12] A. L. Roitburd, Phys. Status Solidi A **37**, 329 (1976); in *Heteroepitaxy of Dissimilar Materials,* edited by R. F. C. Farrow, J. P. Harbison, P. S. Peercy, and A. Zangwill, MRS Symposia Proceedings No. 221 (Materials Research Society, Pittsburgh, 1991).

[13] B. Horovitz, G. R. Barsh, and J. A. Krumhansl, Phys. Rev. B **43**, 1021 (1991).

[14] B. S. Kwak, A. Erbil, B. J. Wilkens, J. D. Budai, M. F. Chisholm, and L. A. Boatner, Phys. Rev. Lett. **68**, 3733 (1992).

[15] L. D. Landau, E. M. Lifshitz, and L. P. Pitaevskii, *Electrodynamics of Continuous Media* (Pergamon, Oxford, 1984), p. 153.

[16] *Thermal Expansion of Nonmetallic Solids,* Vol. 13 of *Thermophysical Properties of Matter,* edited by Y. S. Touloukian, R. K. Kirby, R. E. Taylor, and T. Y. R. Lee (Plenum, New York, 1977).

[17] G. B. Stringfellow, *Organometallic Vapor Phase Epitaxy: Theory and Practice* (Academic, Boston, 1989).

[18] B. S. Kwak, K. Zhang, A. Erbil, B. J. Wilkens, J. D. Budai, M. F. Chisholm, and L. A. Boatner, in Vol. 25 of *Ceramics Transitions, Ferroelectric Thin Films,* edited by A. F. Bhalla and A. S. Nair (American Ceramic Society, Westerville, 1992), p. 212.

[19] B. S. Kwak, K. Zhang, A. Erbil, and B. J. Wilkens, J. Appl. Phys. **69**, 767 (1991).

[20] S. J. Pennycook and D. E. Jesson, Phys. Rev. Lett. **64**, 938 (1990).

[21] L. R. Doolittle, Nucl. Instrum. Methods Phys. Res. Sect. B **9**, 344 (1985).

[22] J. D. Budai, M. F. Chisholm, R. Feenstra, D. H. Lowndes, D. P. Norton, L. A. Boatner, and D. K. Christen, J. Appl. Phys. **58**, 2174 (1991).

[23] S. L. Swartz, D. A. Seifert, G. T. Noel, and T. R. Shrout, Ferroelectrics **93**, 37 (1989).

[24] W. J. Mertz, Phys. Rev. **95**, 690 (1954).

[25] A. F. Devonshire, Philos. Mag. **42**, 1065 (1951); **40**, 1040 (1949).

[26] M. J. Haun, E. Furman, S. J. Jang, H. A. McKinstry, and L. E. Cross, J. Appl. Phys. **62**, 3331 (1987).

[27] J. H. van der Merwe and C. A. B. Ball, in *Epitaxial Growth, Part B,* edited by J. W. Matthews (Academic, New York, 1975), pp. 493–528.

[28] See, for example, S. Timoshenko, *Theory of Elasticity* (MacGraw-Hill, London, 1934), pp. 12–134.

[29] A. G. Khachaturyan, *Theory of Structural Transformations in Solids* (Wiley, New York, 1983), p. 394.

[30] G. Simmons and H. Wang, *Single Crystal Elastic Constants and Calculated Aggregate Properties: A Handbook* (MIT, Cambridge, MA 1971), pp. 210, 280.

[31] H. Uwe and T. Sakudo, J. Phys. Soc. Jpn. **38**, 183 (1975).

[32] D. Freire and R. S. Katiyar, Phys. Rev. B **37**, 2074 (1988).

[33] L. N. Bulaevskii, Fiz. Tverd. Tela (Leningrad) **5**, 3183 (1963) [Sov. Phys. Solid State **5**, 2329 (1964)].

[34] B. S. Kwak, Ph.D. thesis, Georgia Tech, Atlanta, 1992.

[35] S. Wolfram, *Mathematica: A System for Doing Mathematics by Computer* (Addison-Wesley, Redwood City, 1988).

[36] G. A. Rossetti, Jr., L. E. Cross, and K. Kushida, Appl. Phys. Lett. **59**, 2524 (1991).

[37] W. Cao and L. E. Cross, Phys. Rev. B **44**, 5 (1991).

[38] See, for example, J. P. Ansermet, D. Rytz, A. Chatelain, U. T. Hochli, and H. E. Weibel, J. Phys. C **14**, 4541 (1981).

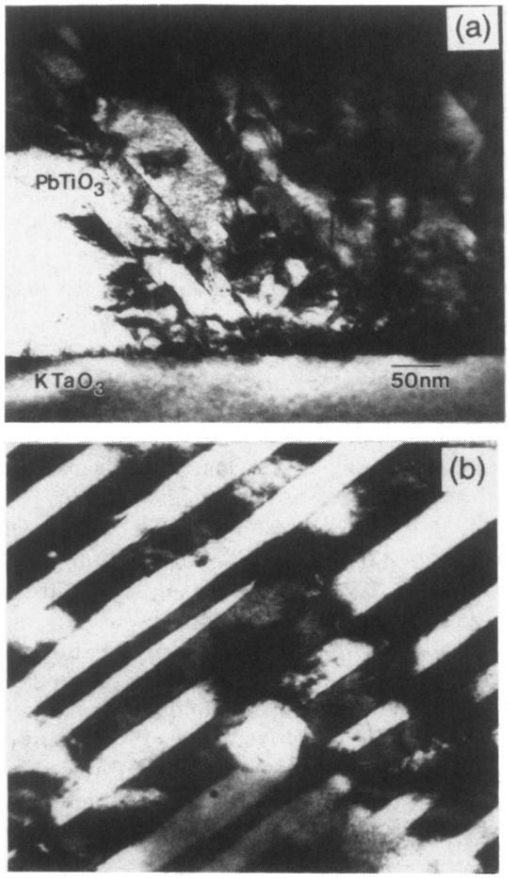

FIG. 7. TEM micrographs showing (a) the domain structure in cross section for a film with a thickness of 450 nm, and (b) the plan view of a film with a thickness of 25 nm. In (b), one can see the directionality of the domain patterns.

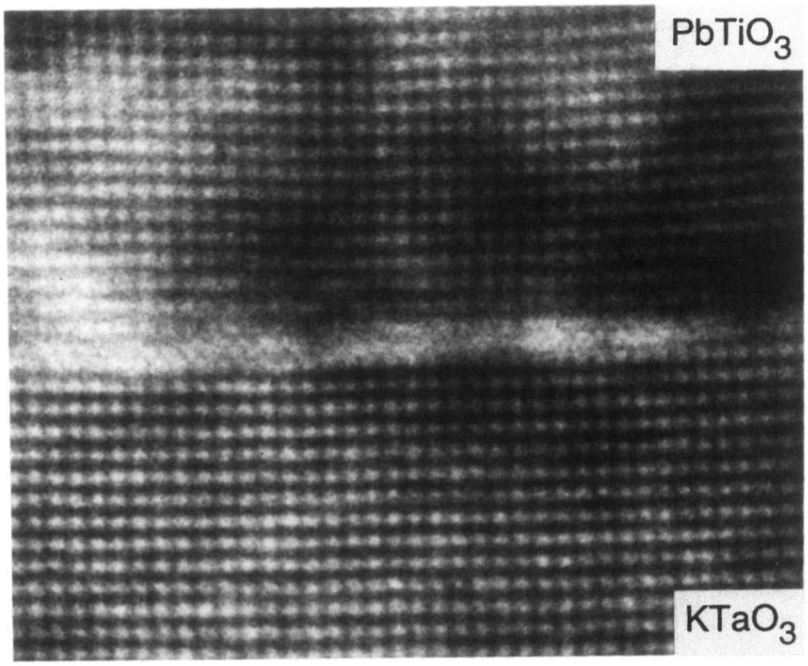

FIG. 8. High-resolution, Z-contrast TEM micrograph for a film with $t = 150$ nm. There are no misfit dislocations in the field of view.